Journal Pre-proofs

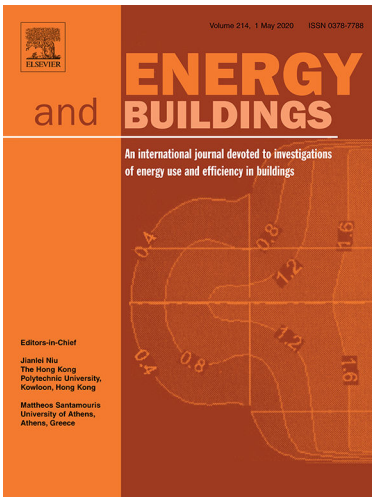

Multi-objective optimization of the refrigerant-direct convective-radiant cooling system considering the thermal and economic performances

Tingting Jiang, Shijun You, Zhangxiang Wu, Huan Zhang, Yaran Wang, Shen Wei

PII: S0378-7788(21)00893-8
DOI: https://doi.org/10.1016/j.enbuild.2021.111609
Reference: ENB 111609

To appear in: *Energy & Buildings*

Received Date: 4 August 2021
Revised Date: 25 September 2021
Accepted Date: 5 October 2021

Please cite this article as: T. Jiang, S. You, Z. Wu, H. Zhang, Y. Wang, S. Wei, Multi-objective optimization of the refrigerant-direct convective-radiant cooling system considering the thermal and economic performances, *Energy & Buildings* (2021), doi: https://doi.org/10.1016/j.enbuild.2021.111609

Multi-objective optimization of the refrigerant-direct convective-radiant cooling system considering the thermal and economic performances

Tingting Jiang [a], Shijun You [a, b], Zhangxiang Wu [a], Huan Zhang [a, b], Yaran Wang [a, b*], Shen Wei [c]

[a] School of Environmental Science and Engineering, Tianjin University, Haihe Education Area, Jinnan District, Tianjin 300350, PR China

[b] Key Laboratory of Efficient Utilization of Low and Medium Grade Energy (Tianjin University), Ministry of Education of China, Tianjin 300350, PR China.

[c] The Bartlett School of Construction and Project Management, University College London (UCL), 1-19 Torrington Place, London WC1E 7HB, United Kingdom.

Abstract

The refrigerant-direct convective-radiant cooling (RCC) system is attracting widespread concern due to its advantages of good thermal comfort, high energy efficiency and simple structure. However, researches on thermal and economic optimization of this system are rare. In this study, a novel heuristic approach is proposed to optimize the aluminum column-wing type refrigerant-direct convective-radiant

* Corresponding author. Tel.: +8602227892626; fax: +8602227892626.

E-mail addresses: yaran_wang@tju.edu.cn

cooling (ACT-RCC) system, which adopts artificial neural network (ANN) integrated with multi-objective genetic algorithm (MOGA). The numerical and economic models of the ACT-RCC terminal are developed and the numerical model is validated by the experimental data. Besides, the ANN model is adopted to accelerate the prediction of the thermal and economic performances of this system. Results show that the training values of the ANN model are fitted well with simulated results and the ANN model can greatly improve the runtime in comparison with original numerical and economic models. Based on the heuristic optimization approach, the optimal structure of the ACT-RCC terminal is the copper pipe diameter with 8.7 mm, copper pipe spacing with 25.5 mm and rib height with 30.3 mm. Compared with original structure, the cooling capacity of the improved ACT-RCC system is enhanced by 16.0% and the initial cost is reduced by 10.0%. The appearance area equals to the direct product of the length and width, and results show that the appearance area of the improved ACT-RCC terminal is decreased from 1.04 m^2 to 0.78 m^2. Therefore, the proposed heuristic approach provides guidance for improving the thermal and economic performances of the RCC systems.

Keywords: refrigerant-direct convective-radiant cooling system; thermal and economic optimization; artificial neural network; multi-objective genetic algorithm;

Nomenclature

A	area (m^2)	γ	correlation degree
b_w	simplified coefficient	φ	relative humidity (%)
c_p	specific heat ($J \cdot kg^{-1} \cdot K^{-1}$)	θ	threshold
D	diameter (m)	ζ	correlation coefficient
f	activation function	***Subscripts***	
G	refrigerant mass flow rate ($kg \cdot s^{-1}$)	aa	appearance area
H	height (m)	al	aluminum-alloy panel
h	convective heat transfer coefficient ($W \cdot m^{-2} \cdot K^{-1}$)	be	building envelope
h_D	conversion heat release coefficient ($W \cdot m^{-2} \cdot K^{-1}$)	co	copper pipe
I	enthalpy ($J \cdot kg^{-1}$)	coi	inner surface of copper pipe
k	number of cases	coo	outer surface of copper pipe
i	node i	e	evaporate
L	length (m)	g	gas
n	number of sections	in	inlet
p	pressure (Pa)	l	liquid
Q	cooling capacity (W)	la	labor
R	goodness of fit	max	maximum value
Sp	spacing (m)	min	minimum value
t	temperature (°C)	n	indoor air
t_m	mean surface temperature (°C)	out	outlet
v	velocity ($m \cdot s^{-1}$)	p	per square meter
w	width (m)	r	refrigerant
w_c	connection weight coefficient	rad	radiation
X	independent variable	se	connection segment
X_i	impact factor	sim	simulated
x	vapor quality	wa	water
x_v	input vector	***Abbreviations***	
y	output vector	ACT-RCC	aluminum column-wing type refrigerant-direct convective-

			radiant cooling
z	shape parameter of rib	ANN	artificial neural network
Δl	control volume length (m)	*AUST*	average uncooled surface temperature
Δp	pressure drop (Pa)	GA	genetic algorithm
Greek symbols		*IC*	initial cost
λ	thermal conductivity ($W \cdot m^{-1} \cdot K^{-1}$)	MOGA	multi-objective genetic algorithm
ε	emissivity	RCC	refrigerant-direct convective-radiant cooling
σ	Stefan-Boltzmann constant, (5.67×10^{-8} $W \cdot m^{-2} \cdot K^{-4}$)		

1. Introduction

According to the International Energy Agency (IEA), the global energy demand is expected to grow by 4.6% in 2021, which exceeds 4% depression in 2020 [1]. It is reported that building industry has become the fourth largest global energy consumer, and accounts for about 21% of the total energy consumption in China [2]. In building energy consumption, half of them is utilized for Heating, Ventilation and Air conditioning (HVAC) systems [3]. Therefore, it is crucial to explore a new technique to reduce energy consumption. The world's first air conditioning system originated in 1902, which can regulate the indoor thermal environment, has been widely used [4]. However, traditional air conditioning systems have the defects of local discomfort and

low energy efficiency due to their heat transfer via forced convection and power consumption of fans.

In recent years, radiant cooling systems exert a significant role in human being's life since they have good thermal comfort and high energy efficiency. In the study of Tian et al. [5], the thermal comfort performance of the radiant ceiling cooling coupled with overhead dedicated outdoor air system was evaluated, and results showed that when the operative temperature was identical, this system could create a more comfortable thermal environment than conventional air conditioning systems. Cen et al. [6] carried out the comparative study between a radiant floor system and a fan coil system, and suggested that the former one possessed its great superiority of the thermal comfort with various space heights. Mikeska et al. [7] developed a simulation model of the radiant cooling system, which was composed of capillary micro tubes and inner plate of sandwich elements, and confirmed that this system had potential in providing good indoor thermal comfort. In the field of research in energy efficiency, Lim et al. [8] established a theoretical model to investigate the dedicated outdoor air system associated with a thermoelectric module radiant cooling panel, and suggested that this system was able to reduce 40.7% of operating energy consumption per year in comparison with conventional variable air volume systems. Kwong et al. [9] compared

the multi-floor radiant slab cooling system and traditional convective air system regarding to energy efficiency, and found that the radiant slab cooling system could save up 34% of energy consumption. An energy simulation method was adopted by Kim et al. [10] to center on the performance of the typical radiant panel system integrated with a decentralized air convector, justifying its contribution to saving energy due to high cooling impact ratio and large coefficient of performance.

The cooling capacity is a pivotal criterion for evaluating the performance of radiant cooling systems. To improve the cooling performance, many scholars have studied the design optimization of radiant cooling systems. Su et al. [11] optimized the heat transfer performance of the radiant cooling ceiling panel system through numerical simulation, illustrating that the cooling panel with thickness of 4.0 ~ 5.0 mm, copper pipe with small diameter and thin plastic join was recommended. Joe et al. [12] put forward a model predictive control strategy to optimize the thermo-economic performance of radiant floor systems, taking the energy consumption and operating cost as objective functions. Results showed that this system could save 29% ~ 50% of energy consumption and 34% of operating cost, comparing to baseline feedback control systems. Ye et al. [13] developed a three-dimensional model to optimize the operating condition of the hybrid cooling system, which integrated the novel free-suspended

ceiling radiant cooling panel with wall attached ventilation system, and results showed that the optimum design was the inlet air velocity of 0.16 $m \cdot s^{-1}$, inlet air temperature of 25 ^{o}C and panel surface temperature of 23 ^{o}C. A multi-objective optimization for a ground source heat pump radiant ceiling air conditioning system was executed by Xie et al. [14], with results showing that compared with conventional parameters, the seasonal performance factor of this system was improved from 3.582 to 3.741 and the operating cost was decreased from 4189.8 $ to 3484.9 $. However, the above radiant cooling systems resist heat by circulating chilled water, which require secondary heat exchange. And these systems need specific plant rooms to place chillers, pumps, water pipes, water collectors etc., with complicated structure. To overcome these obstacles, the RCC system is proposed, which adopts refrigerant as direct circulating medium, and can be designed as split system for individual and flexible application. The RCC system can avoid secondary heat exchange and power consumption of the circulating pump. Moreover, this system has simple structure and is suitable for residential buildings. The authors' previous study adopted the orthogonal design method to improve the structural parameters of the refrigerant-cooling radiant terminal, and results showed that the fin height of 40.0 mm, copper pipe diameter of 6.0 mm, copper pipe spacing of 40.0 mm and aspect ratio of 0.88 were recommended [15]. Nevertheless, the orthogonal design

process is complex and tedious to obtain an optimal design.

The economic performance of radiant cooling systems has also gradually become an attractive research point. The economic indicators have multiple forms, such as net present value, simple payback period and savings to investment ratio. Li et al. [16] adopted cost equations to evaluate the economic efficiency of the radiant cooling terminal and fan coil, and proved that the radiant cooling terminal could make sound economic sense with regard to life cycle. Boccardo et al. [17] used the global cost and payback period to compare the economic performance of three different cooling systems, and results showed that the thermally active building system was the economic choice, the all-air system was the second and the phase change material ceiling panel was the most expensive. Zhou et al. [18] presented that the cooling performance of radiant cooling systems could not be improved blindly, while the cost loss was ignored. Thus, there is a huge challenge to explore not only cooling performance but also initial cost.

The cooling performance and initial cost of the RCC system are interacted with each other. The excessive growth of cooling performance will result in the intense elevation of the initial cost. On the contrary, in order to achieve low initial cost, the cooling performance tends to deteriorate. Therefore, it is essential to exert more efforts

to investigate the trade-off between cooling performance and initial cost. Evaluating the thermal and economic performances of the RCC system requires fast prediction of the performances regarding to various structural parameters. Traditional numerical simulation approaches have large computational burden. The ANN is an efficient method that can accurately and quickly predict the system performance by training with proper data set. Kusiak et al. [19] used the ANN to extract the numerical model of an air handing unit, and then the cooling output is taken as objective function to optimize this system. Ferreira et al. [20] constructed the predictive control model of the HVAC system based on the ANN to achieve good thermal comfort and high energy efficiency. The MOGA can solve multi-objective optimization problem effectively. Imran et al. [21] adopted the MOGA to optimize the hydraulic and thermal performances of the water-to-water chevron type plate heat exchanger, and found a set of optimum solution of pressure drop and heat transfer. A multi-objective optimization based on the MOGA was performed by Bagheri-Esfeh et al. [22] to achieve the minimum cooling and heating loads in a residential building coupled with phase change material.

In order to accelerate the optimization process and improve the accuracy of target value, a novel heuristic approach by combination of the ANN and MOGA is proposed for thermal and economic optimization of the ACT-RCC system. The numerical and

economic models of the ACT-RCC terminal are established and the reliability of the numerical model is validated by the measured data. Then the structural parameters of this terminal including copper pipe diameter, copper pipe spacing and rib height are considered as decision variables, and the cooling capacity and initial cost are chosen as objective functions. Finally, a group of Pareto optimal solutions are obtained and one of them is chosen as optimal target of this terminal.

2. System description

2.1 The *ACT-RCC terminal*

The schematic of the ACT-RCC terminal is shown in Fig. 1, and the key components contain two aluminum-alloy-column panels, four branches copper pipes, cold-storage medium (water), many rectangular fins and one condensation collection plate. Each panel has 10 aluminum-alloy columns and the S-shape copper pipes filled with refrigerant are embedded in the aluminum-alloy columns. Water is chosen as cold-storage medium and sandwiched between copper pipes and aluminum-alloy columns to enhance the cooling capacity, with the weight of 16.0 kg. The rectangular fins are evenly arranged on the backside of the front panel and both sides of the back panel to promote the heat transfer between the ACT-RCC terminal and indoor environment. The

condensation collection plate is located at the bottom of this terminal to collect condensation water. As the ACT-RCC system is designed as split system for decentralized and individual usage, besides, the combined welding operating technology is adopted to ensure the welding quality, the sealing performance is excellent and the risk of refrigerant leakage is low. During the cooling period, the ACT-RCC terminal surface exchanges heat with indoor environment through radiation and natural convection. Then the heat is released to the water and copper pipes successively via heat conduction. Subsequently, the heat is taken away by the refrigerant since the refrigerant evaporates and absorbs heat in copper pipes.

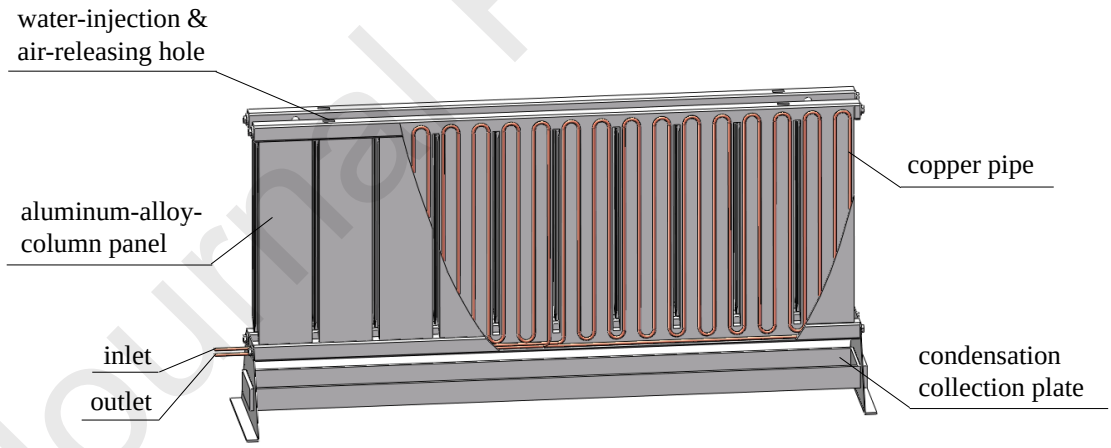

(a) front

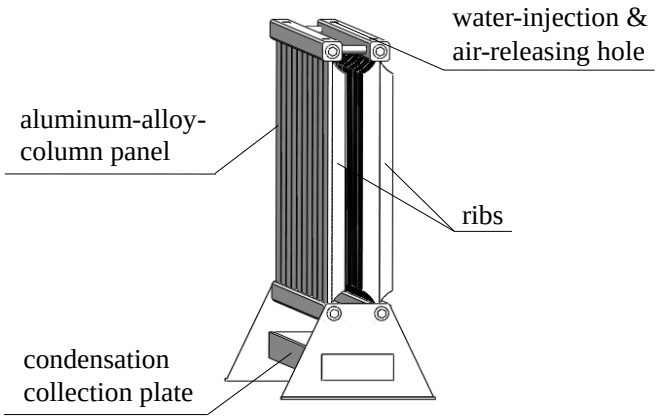

(b) side

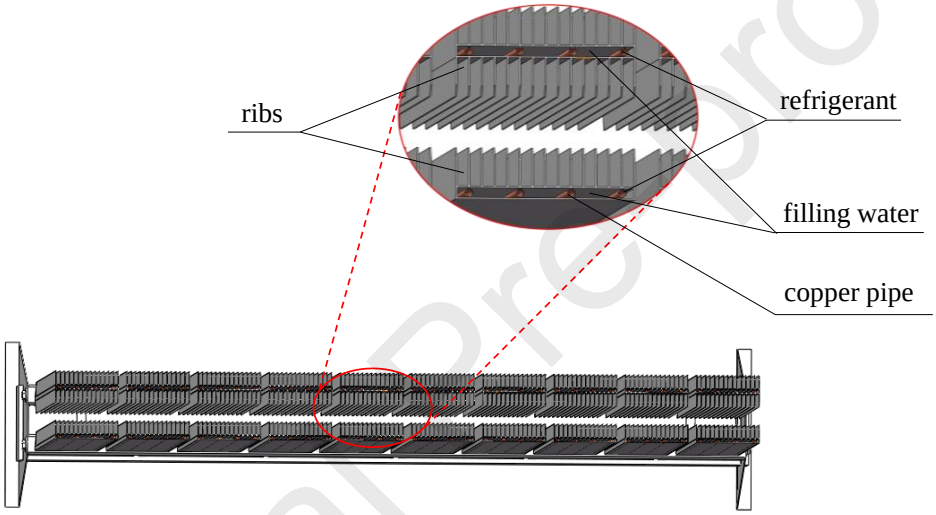

(c) profile

Fig. 1. The schematic of the ACT-RCC terminal.

2.2 Experimental system

The experimental ACT-RCC system is set up in a calorimetric room, as shown in Fig. 2. The key components include two laboratories, one is responsible for simulating indoor environment and the other for simulating outdoor environment, which are

controlled by their independent air conditioning systems. A test room is constructed with steel plate in the indoor environment laboratory to guarantee the heat transfer by natural convection, with the dimension of 3500 mm × 3500 mm × 2500 mm (L × W × H). The main elements of the ACT-RCC system are compressor, gas-liquid separator, four-way valve, condenser, sub-cooler, electronic expansion valve and the ACT-RCC terminal (evaporator), as depicted in Fig. 3. The R410a refrigerant is adopted in this system owing to its ODP with zero. In the test room, the ACT-RCC terminal is arranged 100 mm above the floor and 170 mm away from the wall. According to ASHRAE Standard 55 [23], the measuring point of indoor air temperature is located at the height of 1.1 m in the vertical centerline of the test room to reflect its thermal environment. Correspondingly, the measuring point of indoor relative humidity is also located at this position. During the test, the indoor air temperature is regulated from 26 ^{o}C to 30 ^{o}C and the relative humidity remains 60% constantly. The evaporating temperature is the refrigerant temperature in saturated gas state corresponding to the evaporating pressure at the outlet of the ACT-RRC terminal, and the evaporating temperature of this system is controlled at 6.1 ^{o}C, 8.2 ^{o}C, 9.9 ^{o}C and 11.9 ^{o}C. In order to calculate the cooling capacity of this system under different conditions, the inlet and outlet temperatures and pressures of the ACT-RCC terminal and condenser are measured by K-type

thermocouples and pressure sensors. The refrigerant mass flow rate is recorded by a Coriolis mass flowmeter. The transient response time of the ACT-RCC system is about 26 min due to the existence of water. To ensure that this system is in a stable state, the experimental data is recorded when the system has been running for two hours. The data is collected by the central data acquisition every 2s.

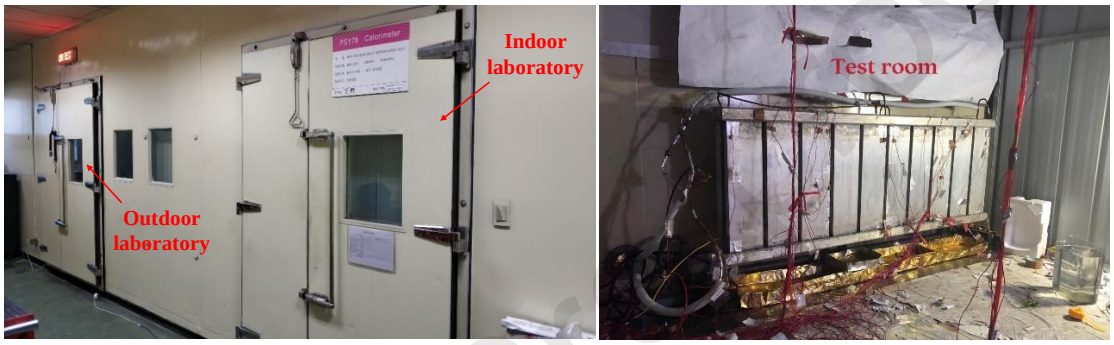

Fig. 2. The picture of the calorimetric room.

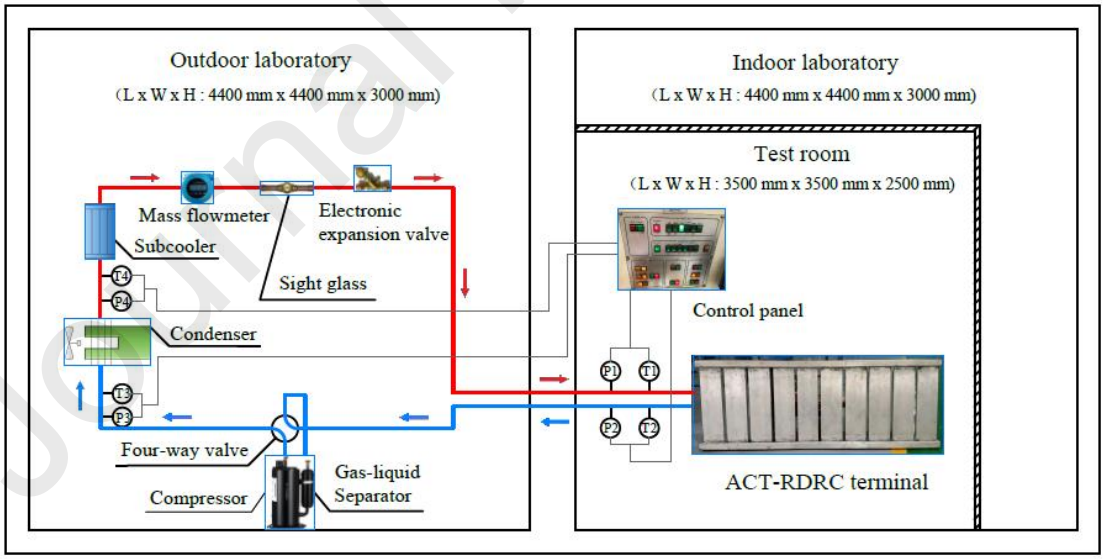

Fig. 3. The experimental ACT-RCC system.

3. Model development

3.1 Numerical model

Due to the composite structure of the ACT-RCC terminal, it is vital to simplify the numerical model reasonably. The following assumptions are as follows:

(1) The heat transfer process of the ACT-RCC terminal is assumed to be one-dimensional and steady-state;

(2) The ACT-RCC terminal is composed of a series of parallel concentric sleeves, and the aluminum-alloy panel can be regarded as a vertical cylinder with the diameter of 11.8 mm.

(3) The heat conduction losses occur in the axial-direction of the refrigerant, copper pipes, water and aluminum-alloy panels are ignored;

(4) The natural convective capacities between water and copper pipes as well as aluminum-alloy columns are extremely petty; therefore, the water in the aluminum-alloy columns is considered as static;

(5) The indoor air temperature and exterior wall temperature remain constant.

The finite volume method is used to simulate the numerical model, and the control volume of each component of the ACT-RCC terminal is exhibited in Fig. 4. The

components are separated into n sections along the refrigerant flow direction, with the length of Δl. The temperatures of the refrigerant, inner and outer surface of the copper pipe, water and aluminum-alloy panel are expressed as t_r, t_{coi}, t_{coo}, t_{wa}, t_{al}, respectively. The energy balance equations for the i th node are given as follows:

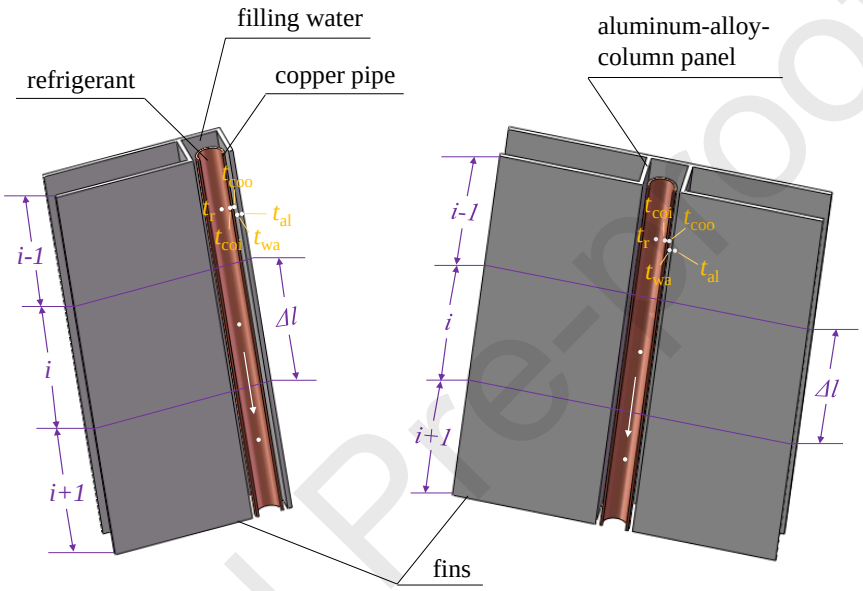

Fig. 4. Sketch of control volumes of the ACT-RCC terminal.

For the refrigerant:

$$G[I_{\text{r-in}}(i)-I_{\text{r-out}}(i)]+\pi D_{\text{r}}\Delta l\cdot h_{\text{r-coi}}(i)[t_{\text{coi}}(i)-t_{\text{r}}(i)]=0,\quad 0<x(i)<1 \tag{1}$$

$$c_{pg}(i)G[t_{\text{r-in}}(i)-t_{\text{r-out}}(i)]+\pi D_{\text{r}}\Delta l\cdot h_{\text{r-coi}}(i)[t_{\text{coi}}(i)-\frac{t_{\text{r-in}}(i)+t_{\text{r-out}}(i)}{2}=0,\quad x(i)=1 \tag{2}$$

$$I_{\text{r}}(i)=x(i)\cdot I_{\text{rg}}(i)+[1-x(i)]\cdot I_{\text{rl}}(i) \tag{3}$$

where G is the refrigerant mass flow rate; $I_{\text{r-in}}$ and $I_{\text{r-out}}$ are the inlet and outlet enthalpies of the refrigerant; D_{r} is the inner diameter of the copper pipe; $h_{\text{r-coi}}$ is the convective heat transfer coefficient between refrigerant and inner surface of the copper pipe; c_{pg} is

the specific heat of the refrigerant in gas phase; $t_{\text{r-in}}$ and $t_{\text{r-out}}$ are the inlet and outlet temperatures of the refrigerant; I_{rg} and I_{rl} are the enthalpies of the refrigerant in gas and liquid phases; x is the vapor quality of the refrigerant, $0 < x < 1$ represents the refrigerant in two phase and $x = 1$ represents the refrigerant in gas phase.

The pressure drop occurs during the refrigerant flows in copper pipes, which is divided into two sections, can be formulated as:

$$\Delta p = \Delta p_{\text{two-phase}} + \Delta p_{\text{gas-phase}} \tag{4}$$

where Δp is the total pressure drop of the refrigerant; $\Delta p_{\text{two-phase}}$ and $\Delta p_{\text{gas-phase}}$ are the pressure drops of the refrigerant in two phase and gas phase.

For the inner surface of the copper pipe:

$$\pi D_{\text{r}} \Delta l \cdot h_{\text{r-coi}}(i)[t_{\text{r}}(i) - t_{\text{coi}}(i)] + \frac{t_{\text{coo}}(i) - t_{\text{coi}}(i)}{\frac{1}{2\pi\lambda_{\text{coi}}} \ln \frac{D_{\text{coo}}}{D_{\text{r}}}} \cdot \Delta l = 0, \quad 0 < x(i) < 1 \tag{5}$$

$$\pi D_{\text{r}} \Delta l \cdot h_{\text{r-coi}}(i)[\frac{t_{\text{r-in}}(i) + t_{\text{r-out}}(i)}{2} - t_{\text{coi}}(i)] + \frac{t_{\text{coo}}(i) - t_{\text{coi}}(i)}{\frac{1}{2\pi\lambda_{\text{coi}}} \ln \frac{D_{\text{coo}}}{D_{\text{r}}}} \cdot \Delta l = 0, \quad x(i) = 1 \tag{6}$$

where λ_{coi} is the thermal conductivity of the copper pipe; D_{coo} is the outer diameter of the copper pipe.

For the outer surface of the copper pipe:

$$\frac{t_{\mathrm{coi}}(i)-t_{\mathrm{coo}}(i)}{\frac{1}{2\pi\lambda_{\mathrm{coi}}}\ln\frac{D_{\mathrm{coo}}}{D_{\mathrm{r}}}}\cdot\Delta l+\frac{t_{\mathrm{wa}}(i)-t_{\mathrm{coo}}(i)}{\frac{1}{2\pi\lambda_{\mathrm{wa}}}\ln\frac{D_{\mathrm{wa}}}{D_{\mathrm{coo}}}}\cdot\Delta l=0 \tag{7}$$

where λ_{wa} is the thermal conductivity of the water; D_{wa} is the diameter of the water.

For the water:

$$\frac{t_{\mathrm{coo}}(i)-t_{\mathrm{wa}}(i)}{\frac{1}{2\pi\lambda_{\mathrm{wa}}}\ln\frac{D_{\mathrm{wa}}}{D_{\mathrm{coo}}}}\cdot\Delta l+\frac{t_{\mathrm{al}}(i)-t_{\mathrm{wa}}(i)}{\frac{1}{2\pi\lambda_{\mathrm{al}}}\ln\frac{D_{\mathrm{al}}}{D_{\mathrm{wa}}}}\cdot\Delta l=0 \tag{8}$$

where λ_{al} is the thermal conductivity of the aluminum-alloy panel; D_{al} is the diameter of the aluminum-alloy panel.

For the aluminum-alloy panel:

$$\begin{aligned}&\frac{t_{\mathrm{wa}}(i)-t_{\mathrm{al}}(i)}{\frac{1}{2\pi\lambda_{\mathrm{al}}}\ln\frac{D_{\mathrm{al}}}{D_{\mathrm{wa}}}}\cdot\Delta l+Q_{\mathrm{rad,al\text{-}be}}(i)+\frac{h_{\mathrm{air}}(i)}{c_{p\text{-air}}}[I_{\mathrm{air}}-I_{\mathrm{al}}(i)]\\&\cdot(\pi D_{\mathrm{al}}\Delta l+w_{\mathrm{se}}\Delta l\cdot 2)+\frac{2h_D(I_{\mathrm{air}}-I_{\mathrm{rib}})}{b_w}\cdot\frac{th(z\Delta l)}{z}\cdot 2=0\end{aligned} \tag{9}$$

where h_{air} is the natural convective heat transfer coefficient; $c_{p\text{-}air}$ is the specific heat of air; I_{air} is the enthalpy of air; I_{al} is the enthalpy of the saturated air boundary layer on aluminum-alloy panel; w_{se} is the width of the connection segment; h_{D} is the conversion heat release coefficient of air side on rib surface; I_{rib} is the enthalpy of the saturated air boundary layer on rib surface; b_w is the simplified coefficient of air enthalpy; z is the shape parameter of the rib; $Q_{\mathrm{rad,al\text{-}be}}$ is the radiant heat transfer between aluminum-alloy

panel and building envelopes, which can be expressed as:

$$Q_{\text{rad,al-be}} = \varepsilon \cdot \sigma \cdot A_{\text{al}}[(t_{\text{m}} + 273.15)^4 - (AUST + 273.15)^4] \tag{10}$$

$$AUST = \frac{\sum_{i=1}^{n} A_i t_i}{\sum_{i=1}^{n} A_i} \tag{11}$$

where ε is the emissivity; σ is the Stefan-Boltzmann constant, $5.67 \diamond 10^{-8}$ W· m^{-2}· K^{-4}; A_{al} is the area of the aluminum-alloy panel; t_{m} is the mean surface temperature of the aluminum-alloy panel; *AUST* is the average uncooled surface temperature of building envelopes; A_i and t_i are the area and temperature of each enclosure.

Therein, the correlations of $h_{\text{r-coi}}$, Δp and h_{air} of the numerical model can be obtained in Ref. [24-26].

3.2 Economic model

The economic model is established to evaluate the economic performance of the ACT-RCC system. As the outdoor unit of this system is the same as that of traditional split air-conditioners, only the initial cost (*IC*) of the ACT-RCC terminal is calculated. The *IC* is made up of the aluminum-alloy panels cost (IC_{al}), ribs cost (IC_{rib}), copper pipes cost (IC_{co}) and labor cost (IC_{la}). Therefore, the *IC* is defined as follow:

$$IC = IC_{al} + IC_{rib} + IC_{co} + IC_{la} \quad (12)$$

The IC_{al}, IC_{rib} and IC_{co} can be determined using the following equations:

$$IC_{al} = IC_{p\text{-}al} \cdot A_{al} \quad (13)$$

$$IC_{rib} = IC_{p\text{-}rib} \cdot A_{rib} \quad (14)$$

$$IC_{co} = IC_{p\text{-}co} \cdot L_{co} \quad (15)$$

where $IC_{p\text{-}al}$ and $IC_{p\text{-}rib}$ are the prices per square meter of the aluminum-alloy-column panel and rib; A_{al} and A_{rib} are the areas of the aluminum-alloy-column panel and rib; $IC_{p\text{-}co}$ is the price per meter of copper pipes and L_{co} is the length of copper pipes.

The prices of the copper pipe with different diameters, aluminum-alloy material and labor cost are displayed in Table 1.

Table 1. The prices of different materials of the ACT-RCC terminal [15, 27].

Category	Prices	Category	Diameter (mm)	Prices
aluminum-alloy panel	10.0 $\$\cdot m^{-2}$	copper pipe	4.0	0.5 $\$\cdot m^{-1}$
			5.0	0.9 $\$\cdot m^{-1}$
			6.35	1.0 $\$\cdot m^{-1}$
			8.0	1.5 $\$\cdot m^{-1}$
rib	6.6 $\$\cdot m^{-2}$		9.52	1.6 $\$\cdot m^{-1}$
			10.0	2.1 $\$\cdot m^{-1}$
labor cost	14.8 $		12.0	2.3 $\$\cdot m^{-1}$
			14.0	3.5 $\$\cdot m^{-1}$

3.3 Optimization model

Optimizing the thermal and economic performances of the ACT-RCC system requires numerical solution of the proposed numerical and economic models, of which the computational burden is very extensive. In order to accelerate the performance prediction process, the ANN model is adopted to regress the input-output simulated data of the ACT-RCC system.

3.3.1 ANN model

The ANN is a kind of mathematical model, which adopts the structure similar to synaptic connection of brain to process information [28]. The ANN is composed of a large number of nodes (or neurons) and connection sections. The connection between two nodes represents the weighted value of signal passing through this interface, called weight, which is equivalent to the memory of the ANN. The common multilayer neural network is made up of input layer, output layer and hidden layer. The purpose of neural network is to learn from the environment by adjusting its neuron weight and threshold until the output error achieves the expected value. Many researchers have adopted the ANN model for predicting the thermal performance of absorption heat pump systems [29], air conditioning systems [30] and liquid desiccant systems [31].

The mathematical model of the artificial neuron is shown in Fig. 5. The information of input layer is named as input vector. Correspondingly, the information of output layer is named as output vector. The correlation between input vector and output vector in the ANN model can be expressed as:

$$y_i = f\left(\sum_{i=1}^{n} w_{c,i} \cdot x_{v,i} - \theta\right) \tag{16}$$

where x_v is the input vector; y is the output vector; w_c is the connection weight coefficient; θ is the threshold of the hidden layer neural node; f is the activation function, which depends on neurons output.

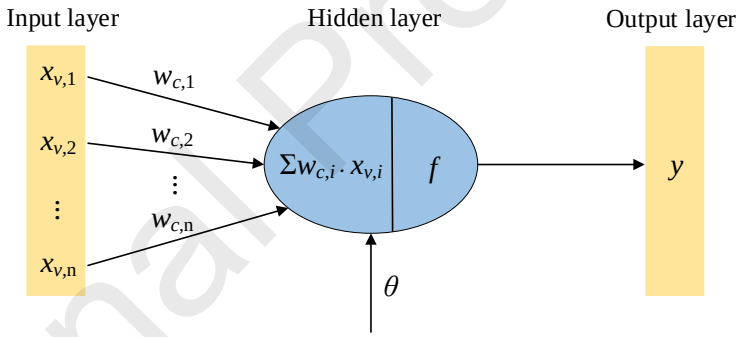

Fig. 5. The mathematical model of the artificial neuron [32].

In this work, the ANN model is developed to predict the correction between structural parameters and thermal and economic performances of the ACT-RCC system, as displayed in Fig. 6. The input variables are copper pipe diameter, copper pipe spacing and rib height, and the output objectives are cooling capacity and initial cost. The training process is to achieve minimum gap between ANN output and correct output by

adjusting weight and deviation coefficient.

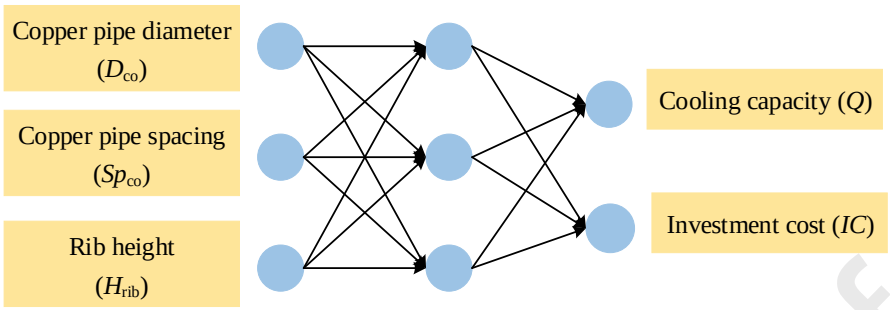

Fig. 6. The ANN model of the ACT-RCC system [30].

3.3.2 MOGA optimization

The genetic algorithm (GA) is a method to search the optimal solution through simulating the natural evolution process, which originates from the computer simulation of biological system [33]. GA encodes the problem parameters as chromosomes, and then uses iterative process for selection, crossover and mutation to exchange the population chromosome information, and finally produces the fittest target chromosome. The flow chart of the GA for optimization process is depicted in Fig. 7. In terms of single objective problem, the GA has its own obvious superiority and practical value. In terms of multi-objective optimization problem, the non-dominated sorting genetic algorithm-II (NSGA-II) is the most widely applied [34]. However, each objective function of the NSGA- II is in conflict with each other, and one target improves may cause the performance depression of another. It is difficult to achieve the

optimal solution of all objective functions simultaneously. Thus, the means of coordination and compromise are adopted to overcome this issue, and then the Pareto optimal solution set is derived. Many scholars have successfully utilized the NSGA- II to obtain the optimal target of the porosity and thermal diffusivity of fluid [35], green building design [36] and HAVC system control [37].

The MOGA is employed to optimize the thermal and economic performances of the ACT-RCC system. The cooling capacity and initial cost are chosen as objective functions. The structural parameters of the copper pipe diameter, copper pipe spacing and rib height are selected as decision variables, and their scopes are exhibited in Table 2.

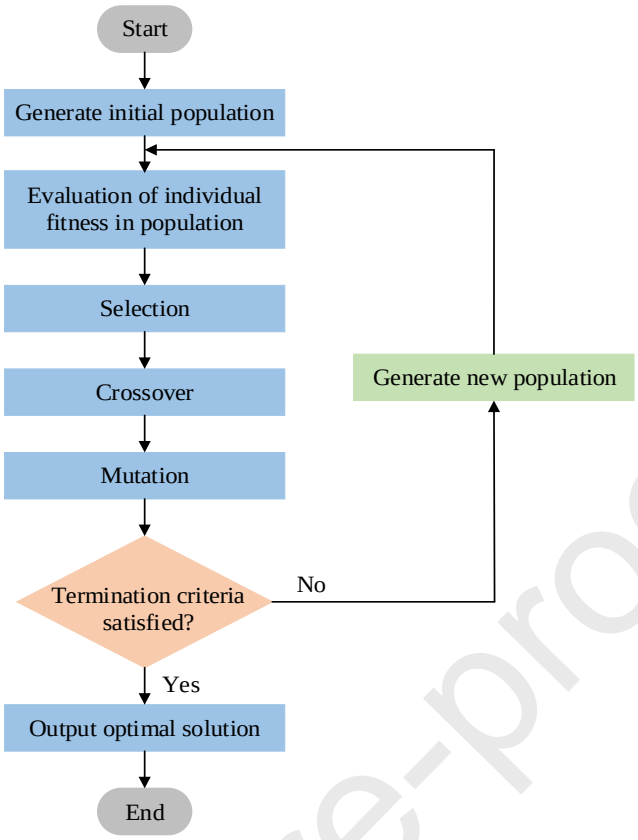

Fig. 7. Flow chart of genetic algorithm optimization process [4].

Table 2. The ranges of decision variables for optimization.

Decision variables	Ranges	Unit
copper pipe diameter (D_{co})	5.0 ~ 14.0	mm
copper pipe spacing (Sp_{co})	20.0 ~ 100.0	mm
rib height (H_{rib})	5.0 ~ 50.0	mm

3.4 Solution strategy

The simulated calculation and optimization of the ACT-RCC system are based on Python environment, and the solution procedure is presented in Fig. 8. The solution

steps are as follow: (a) input operating parameters and environmental parameters, and then calculate the cooling capacity by iterative method; (b) input structural parameters to calculate the *IC* based on the economic model; (c) select the data sets for training neural network to correlate between decision variables and objective functions using the ANN model; (d) determine the lower and upper bound of each decision variable, and then adopting the MOGA to perform optimization operation; (e) output Pareto optimal solution.

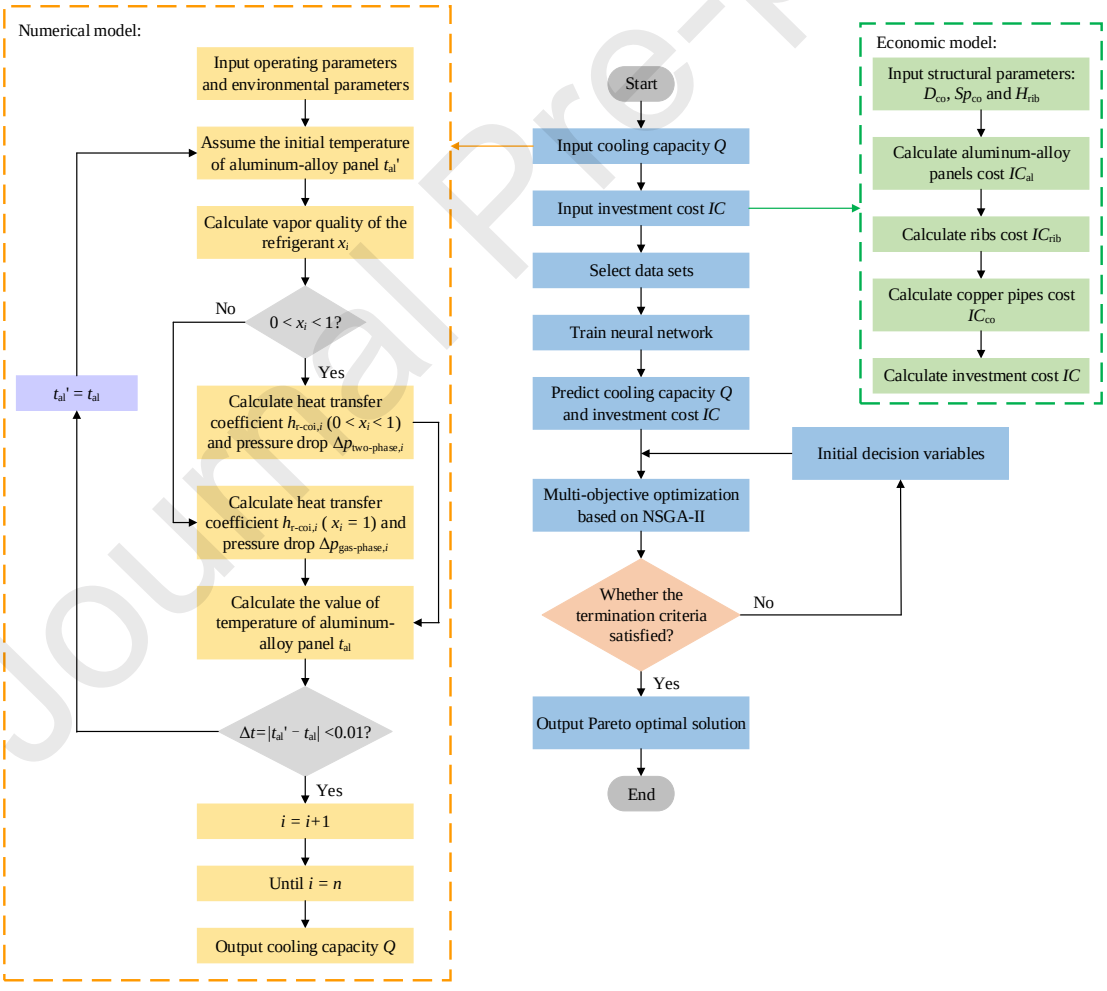

Fig. 8. Optimization framework of the ACT-RCC system.

3.5 Model validation

The geometrical parameters of the ACT-RCC terminal are listed in Table 3. The measured data including refrigerant mass flow rate (G), inlet pressure (p_{in}) and temperature (t_{in}) of the ACT-RCC terminal as well as indoor air temperature (t_n) and relative humidity (φ), velocity (v) are used as input parameters. The tested and simulated results of the outlet pressure (p_{out}) and temperature (t_{out}) of the ACT-RCC terminal are depicted in Table 4, and their cooling capacities are compared in Fig. 9. Case 1 ~ 4 display the variation trends of the outlet pressure and temperature as well as cooling capacity under the evaporating temperature (t_e) of 6.1 ºC ~ 11.9 ºC, with the indoor air temperature at 26 ºC. Cases 5 ~ 8 and Cases 9 ~ 12 reflect its properties with the indoor air temperature at 28 ºC and 30 ºC. It is found that the deviations of the outlet pressure and temperature between simulated and measured data vary from 0.2×10^6 Pa ~ 0.3×10^6 Pa and 0.5 ºC ~ 1.3 ºC, and the relative error of the cooling capacity is within the range of 1.5% ~ 6.7%. The simulated results exhibit reasonable agreement with the experimental data, indicating the reliability of the established numerical model of the ACT-RCC terminal.

In addition, the accuracy of the constructed ANN model of the ACT-RCC system is evaluated by numerous simulated data. The data sets of the cooling capacity are

divided into two groups. The first 50 data sets are selected for training neural network, and the other 10 data sets are used for validation. Correspondingly, the same number of data sets are distributed for initial cost. The simulated and predicted results of the cooling capacity and initial cost based on the ANN model are displayed in Fig. 10. It can be observed that the predicted values are in accordance with the simulated data for both cooling capacity and initial cost, and the goodness of fit are 0.9854 and 0.9631. The computer used for simulation has an Intel(R) Core (TM) i5-6500 64bit CPU and 8.00GB RAM memory. The runtimes of the original numerical and economic models as well as the ANN model of the ACT-RCC terminal are separately compared in Table 5. It is indicated that the runtimes of the ANN model are extremely short, which merely take 1.21 s for cooling capacity and 1.24 s for initial cost. Therefore, the established ANN model can be used to accurately and quickly predict the thermal and economic performances of the ATC-RCC system.

Table 3. The geometrical parameters of the ACT-RCC terminal.

Components	Dimension (mm)	Components	Diameter (mm)
ACT-RCC terminal	1600 × 100 × 650 (L × W × H)	inner surface of copper pipe	5.35
rib spacing	10.0	outer surface of copper pipe	6.35
rib height	20.0	water	11.55
copper pipe spacing	40.0	aluminum-alloy panel	11.80

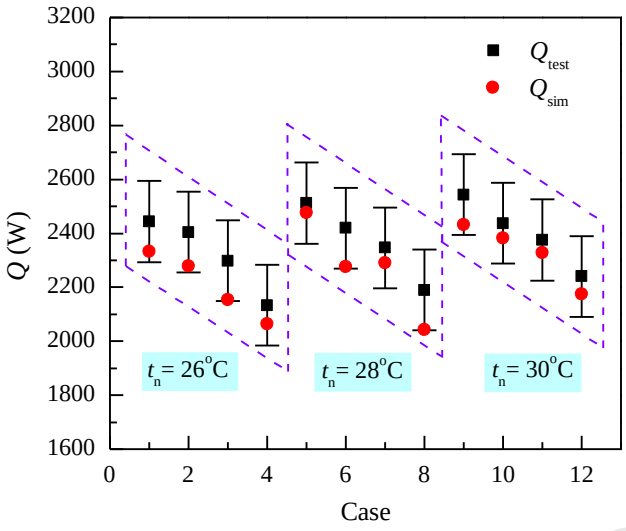

Fig. 9. Comparisons of the tested and simulated cooling capacity.

Table 4. Comparisons of the experimental data and simulated results of the ACT-RCC system.

Parameters	Case 1	Case 2	Case 3	Case 4	Case 5	Case 6	Case 7	Case 8	Case 9	Case 10	Case 11	Case 12
t_n (°C)	26.0	26.0	26.0	26.0	28.0	28.0	28.0	28.0	30.0	30.0	30.0	30.0
t_e (°C)	6.1	8.2	9.9	11.9	6.1	8.2	9.9	11.9	6.1	8.2	9.9	11.9
G (kg·s^{-1})	53.0	51.8	49.0	47.3	53.9	52.0	49.9	47.8	54.3	52.5	50.6	48.5
p_{in} ($\times 10^6$ Pa)	9.7	10.2	10.7	11.2	9.7	10.3	10.8	11.3	9.7	10.3	10.8	11.3
t_{in} (°C)	7.0	8.3	9.5	10.2	7.0	8.7	10.0	10.7	6.8	9	10.3	11.2
$p_{out,\ test}$ ($\times 10^6$ Pa)	9.6	10.2	10.7	11.4	9.6	10.3	10.8	11.5	9.6	10.3	10.8	11.5
$p_{out,\ sim}$ ($\times 10^6$ Pa)	9.4	9.9	10.4	11.1	9.3	10.0	10.5	11.2	9.3	10.1	10.5	11.2
$t_{out,\ test}$ (°C)	13.9	14.7	15.3	16.2	15.4	15.6	16.5	16.9	15.8	16.6	17.3	17.6
$t_{out,\ sim}$ (°C)	13.3	14.1	14.6	15.5	14.9	15.0	15.9	16.5	14.5	16.1	16.6	17.0

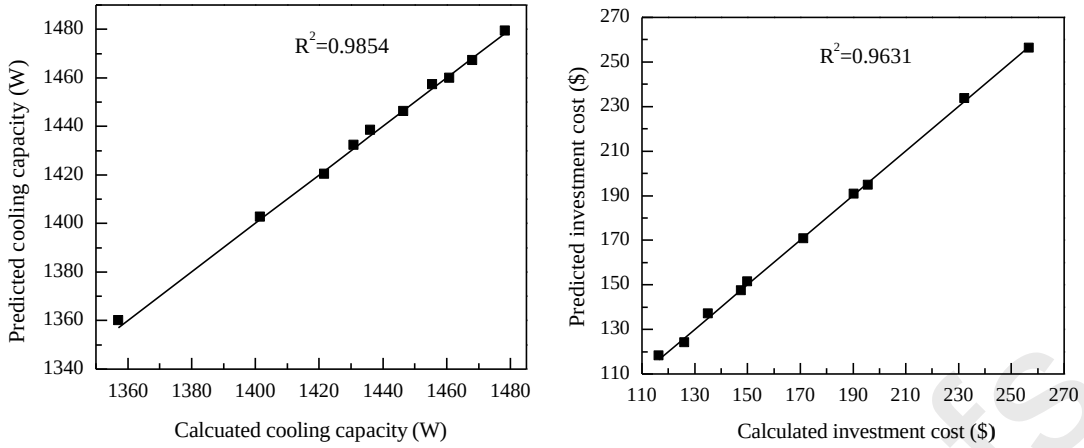

(a) cooling capacity (b) initial cost

Fig. 10. The simulated and predicted values based on the ANN model.

Table 5. The runtimes of the original numerical and economic models as well as the ANN model.

Parameters	Original numerical/economic model runtime (s)	ANN model runtime (s)
cooling capacity (*Q*)	2250.6	1.21
initial cost (*IC*)	6.5	1.24

4. Results and discussion

In this section, the impacts of different structural parameters on thermal and economic performances of the ATC-RCC system are examined comprehensively based on the numerical and economic models. Subsequently, the sensitivity of the above factors is analyzed. Then the combination of the ANN model and MOGA is applied to search the optimal structure of the ATC-RCC terminal. Finally, the thermal and economic performances of the improved ATC-RCC system is further compared with

other structures. The values of operating parameters and environmental parameters used for simulation are depicted in Table 6.

Table 6. The operating parameters and environmental parameters of the ACT-RCC system.

Operating parameters	Values	Environmental parameters	Values
G (kg· s^{-1})	8.3 ×10^{-3}	t_n (°C)	26.0
I_r (J· kg^{-1})	2.6 ×10^5	φ (%)	60.0
t_{in} (°C)	8.3	v (m· s^{-1})	0.2
p_{in} (Pa)	1.02 ×10^6		
Δl (m)	0.05		

4.1 Impact factor on thermal and economic performances

4.1.1 Copper pipe diameter

Different copper pipe diameters (D_{co}) are used in the numerical and economic models to explore its effect on thermal and economic performances of the ACT-RCC system, in the premise of copper pipe spacing (Sp_{co}) with 40.0 mm and rib height (H_{rib}) with 20.0 mm. Fig. 11 depicts the change of the cooling capacity (Q) with the increase of the D_{co}. When the D_{co} rises from 5.0 mm to 14.0 mm, the refrigerant outlet superheat decreases approximately 1.5 °C, as shown in Fig. 12. Then the refrigerant outlet temperature is dropped from 19.9 °C to 18.5 °C, resulting in the reduction of the mean

surface temperature of the ACT-RCC terminal and the improvement of the Q. Meanwhile, the IC is improved significantly by 4.7% ~ 82.2%, which is mainly attributed to the enhancement of the IC_{co} with large D_{co} even though the length of copper pipes (L_{co}) declines. In addition, as the D_{co} varies from 5.0 mm to 10.0 mm, the average growth rate of the Q is 1.2 W, while it drops to 0.03 W when the D_{co} is larger than 10.0 mm. Correspondingly, the average growth rate of the IC is 10.1 $ firstly, and then climbs to 18.5 $. It indicates that the excessive increase of the D_{co} (over 10.0 mm) will lead to the decrease of the increment of the Q and the elevation of the IC. Therefore, the D_{co} with 5.0 ~ 10.0 mm is a great option for optimization of the ACT-RCC terminal.

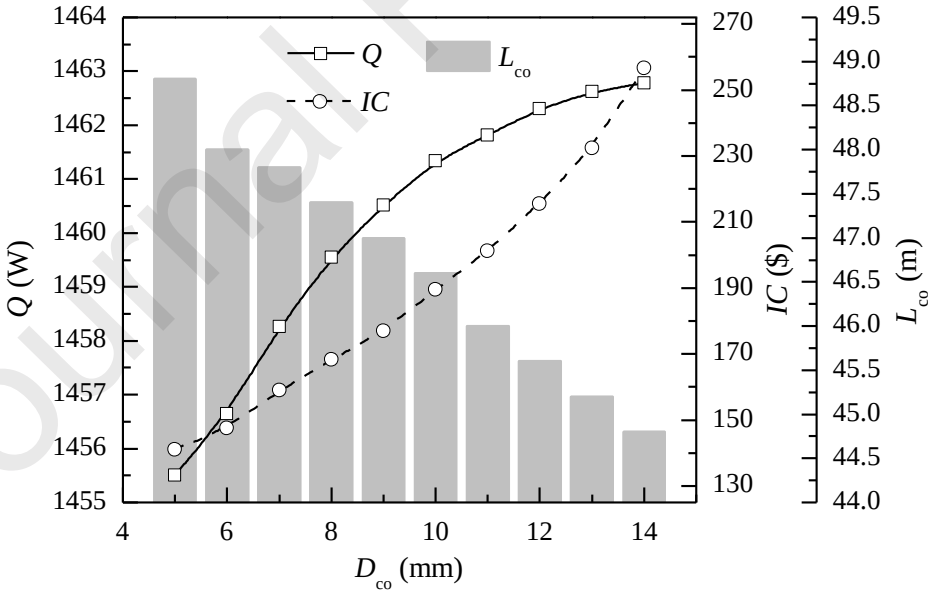

Fig. 11. Effect of D_{co} on thermal and economic performances of the ACT-RCC system.

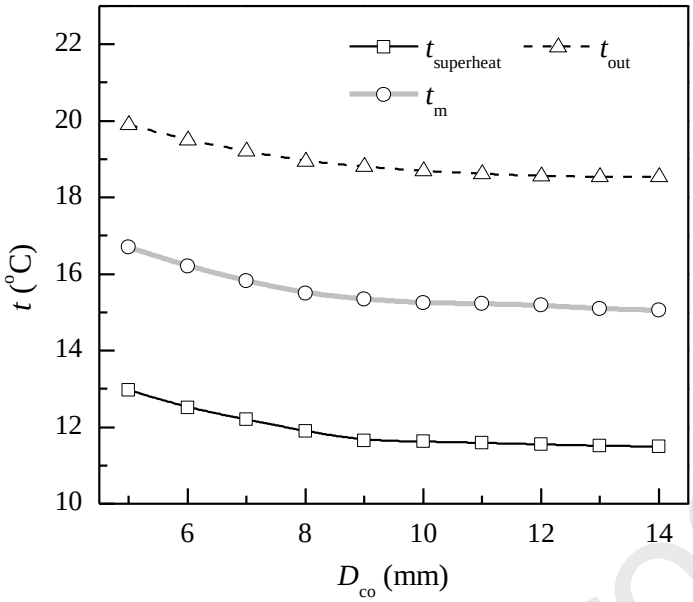

Fig. 12. Different temperature variations under various D_{co}.

4.1.2 Copper pipe spacing

The change of the Sp_{co} exerts a significant role in evaluating the thermal and economic performances of the ACT-RCC system. In order to elucidate the relationship among them, the D_{co} and H_{rib} are remained 5.0 mm and 20.0 mm. Results presented in Fig. 13 show that as the Sp_{co} increases from 20.0 mm to 100.0 mm, the Q is decreased by 0.2% ~ 3.6%. This is due to the reduction of the L_{co}, ranging from 54.6 m to 35.4 m. However, the IC ascends from 143.0 $ to 154.3 $ owing to the enhancement of the aluminum-alloy panel area, that is to say, the rising rate of the IC_{al} is superior to the dropping rate of the IC_{co}. It is noted that the less Sp_{co} leads to the higher Q and the lower IC, as a consequence, the copper pipes with small spacing of the ACT-RCC terminal is

recommended in the following simulation.

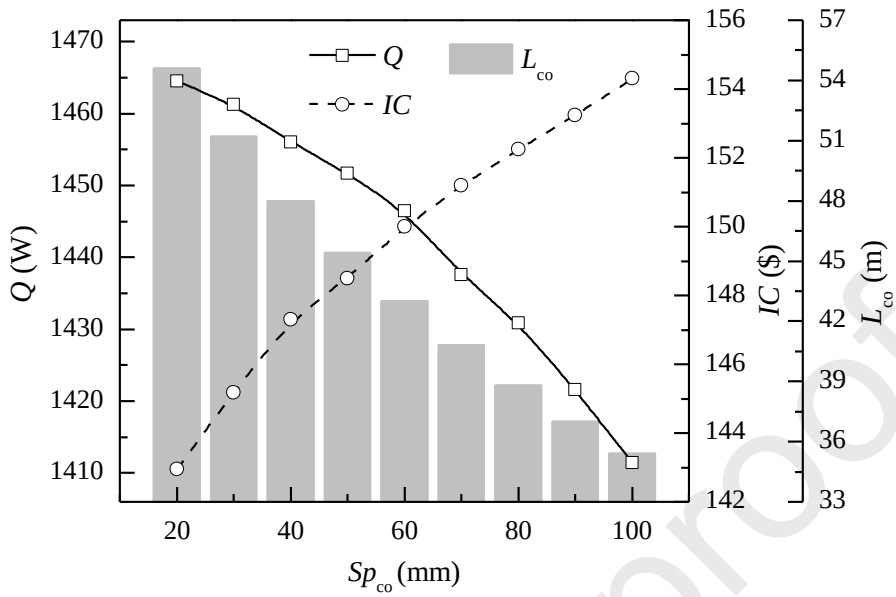

Fig. 13. Effect of Sp_{co} on thermal and economic performances of the ACT-RCC system.

4.1.3 Rib height

The thermal and economic performances of the ACT-RCC system are limited by different H_{rib}, as well. Fig. 14 depicts the variations of the Q and IC against the H_{rib} with the D_{co} of 5.0 mm and Sp_{co} of 40.0 mm. It can be found that both the Q and IC are descended with the increase of the H_{rib} since the L_{co} decreases from 103.6 m to 23.2 m. As the H_{rib} changes from 35.0 mm to 50.0 mm, the Q drops intensely with the average descent rate of 6.3%, which is much greater than that of the H_{rib} between 5.0 mm and 35.0 mm. This phenomenon can be explained that the refrigerant outlet state of the ACT-RCC terminal is two-phase, that is, the refrigerant is not completely evaporated

due to the excessively diminution of the L_{co}. As shown in Fig. 15, when the H_{rib} is larger than 35.0 mm, the vapor quality is decreased obviously from 1.0 to 0.87. Correspondingly, the t_{out} and $t_{superheat}$ vary slightly. Therefore, the H_{rib} within the range of 5.0 mm ~ 35.0 mm is determined for optimizing the ACT-RCC terminal.

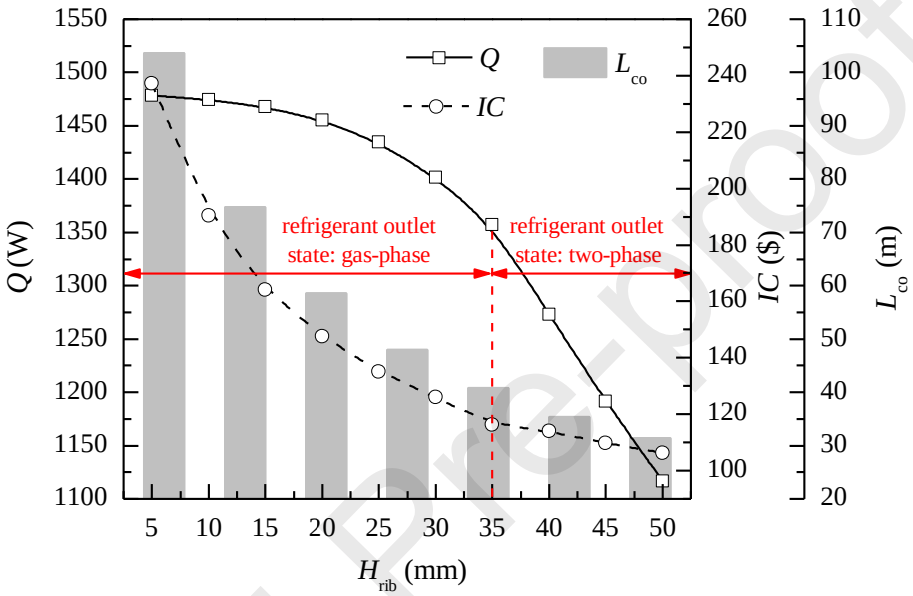

Fig. 14. Effect of H_{rib} on thermal and economic performances of the ACT-RCC system.

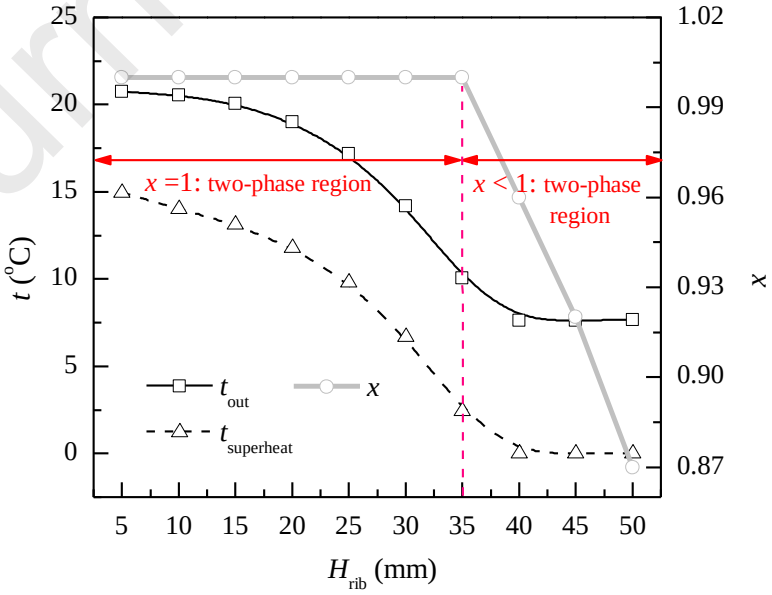

Fig. 15. Different temperatures and vapor quality variations under various H_{rib}.

4.1.4 Grey relational analysis on impact factors

Grey relational analysis reflects the correlation degree in the developing process of two objects based on the grey system analysis, prediction and decision-making. If the synchronous change ratios of two impact factors are high, it indicates that they possess superior relevance and vice versa. In this section, the correlation degrees among the different structural parameters and *Q* as well as *IC* of the ACT-RCC system are conducted by grey relational analysis. Firstly, the original data sequence should be processed in dimensionless treatment, and its expression is written as:

$$X_0' = \frac{X_0}{x_0(1)} = (x_0'(1), x_0'(2), \cdots, x_0'(k)), \quad k = 1, 2, \cdots, 50 \tag{17}$$

$$X_i' = \frac{X_i}{x_i(1)} = (x_i'(1), x_i'(2), \cdots, x_i'(k)), \quad i = 1, 2, 3 \tag{18}$$

where X_0 is the cooling capacity or initial cost of the ACT-RCC system; X_i is the value of the impact factor; k is the number of cases.

Then the correlation coefficient of the impact factor can be calculated according to Eq. (19):

$$\zeta_{0i}(k) = \frac{\Delta_{\min} + 0.5\Delta_{\max}}{\Delta_{0i}(k) + 0.5\Delta_{\max}} \tag{19}$$

$$\Delta_{0i}(k) = \left| x_0(k) - x_i(k) \right| \tag{20}$$

$$\Delta_{\max} = \max_i \max_k \left| x_0(k) - x_i(k) \right| \tag{21}$$

$$\Delta_{\min} = \min_i \min_k \left| x_0(k) - x_i(k) \right| \tag{22}$$

Finally, the correlation degree of the impact factor is evaluated based on the correlation coefficient, which is defined as:

$$\gamma_{0i} = \frac{1}{k}(\zeta_{01}(1) + \zeta_{01}(2) + \cdots \zeta_{01}(k)) \tag{23}$$

where γ is the correlation degree of the impact factor.

The results of grey relational analysis of the structural parameters are presented in Table 7. With regard to *Q*, the crucial relevant factor is the H_{rib} with the correlation degree of 0.913. The grey correlation of these factors is ordered as: $H_{\text{rib}} > Sp_{\text{co}} > D_{\text{co}}$, indicating that the H_{rib} contributes significantly to cooling performance of the ACT-RCC system. With regard to *IC*, the D_{co} is a dictator and its correlation degree is 0.767. The influence degree of these factors is sorted as: $D_{\text{co}} > H_{\text{rib}} > Sp_{\text{co}}$. It can be denoted that the D_{co} exerts a prominent role in initial cost of this system.

Table 7. Gray correlation analysis of structural parameters.

Structural parameters	Correlation degrees	
	cooling capacity (*Q*)	initial cost (*IC*)
copper pipe diameter (D_{co})	0.820	0.767
copper pipe spacing (Sp_{co})	0.864	0.694
rib height (H_{rib})	0.913	0.751

4.2 Optimization results

The Pareto optimal solutions of optimization for the ACT-RCC system are exhibited in Fig. 16. The primary target of this study is to explore maximum *Q* and minimum *IC*. While the default values of all objective functions are of the minimum type, thus the *Q* can be replaced by -*Q*. Then totally 23 solutions are derived. It can be observed that the improvement of the *Q* within the range of 1478.9 W ~ 1745.5 W resulting in the elevation of the *IC* within the range of 17.4 $~ 149.0 $. When the *IC* is chosen as the single objective function, point A can be taken as the preferred answer with the minimum value of 21.6 $ while the corresponding *Q* is the lowest. On the contrary, when the *Q* is a main priority, point B provides the best solution with the maximum value of 1745.5 W whereas the *IC* will be sacrificed.

In the MOGA, all the results from the Pareto front can be used as the optimal solution. However, only one solution should be selected as the best project in practical application. The technique for order preference by similarity to an ideal solution (TOPSIS) is a general decision-making method to settle this issue, and the ideal and non-ideal points need to be identified at first [38]. The ideal point is defined as the optimal value of each target, on the contrary, is non-ideal point. The optimal point is located at the nearest distance from the ideal point and the farthest distance from the

non-ideal point [39]. In Fig. 16, the results illustrate that the optimal solution of the ACT-RCC system is associated with the Q of 1688.3 W and IC of 132.9 $, which is denoted by point C. The corresponding values of the decision variables are listed in Table 8.

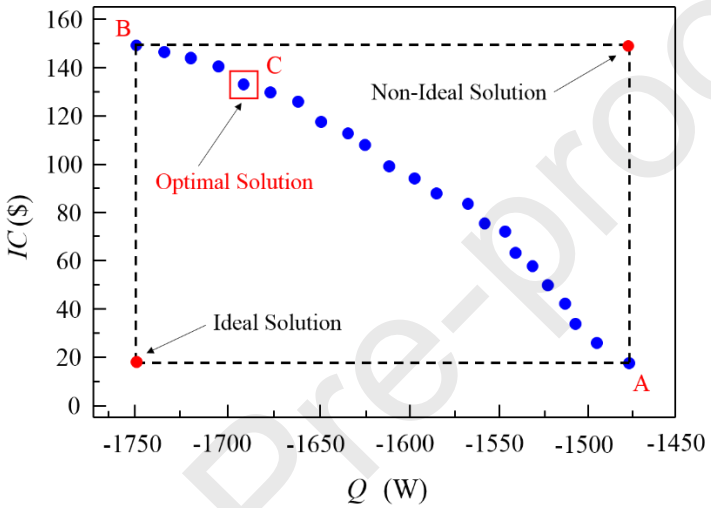

Fig. 16. Pareto optimal solutions of the MOGA.

Table 8. The optimization results of the ACT-RCC terminal.

Project	Parameters	Values	Unit
Decision variables	copper pipe diameter (D_{co})	8.7	mm
	copper pipe spacing (Sp_{co})	25.5	mm
	rib height (H_{rib})	30.3	mm
Objective functions	cooling capacity (Q)	1688.3	W
	initial cost (IC)	132.9	$

4.3 Comparison with other structures

The cooling capacity per unit appearance area (Q_{aa}) is introduced to evaluate the cooling performance since the appearance areas of the RCC terminal with different structures are diverse. The Q_{aa} and *IC* of the optimum solution of the ACT-RCC system are compared with its original structure, as shown in Table 9. It turns out that the Q_{aa} of the improved ACT-RCC system is increased by 16.0% and the *IC* is declined by 9.9%. This is due to the reduction of the L_{co} and the increment of the aluminum-alloy panels and ribs areas, leading to the enhancement of the Q_{aa} and the depression of the *IC*. Furthermore, both the appearance areas are also compared. Results show that the appearance area of the improved ACT-RCC terminal is less than the original structure, which is 1200 mm (L) × 650 mm (H), indicating that this terminal has great potential in saving occupation area. It can be concluded that the proposed heuristic optimization approach of the combination of the ANN and MOGA is beneficial for improving the thermal and economic performances of the RCC system.

In addition, a comparison between the improved ACT-RCC terminal and the improved steel-panel RCC terminal has been performed to evaluate their advantages regarding to thermal and economic performances as well as occupation area. Results presented in Table 9 show that the optimal results of the steel-panel RCC terminal are

the Q_{aa} of 109.8 W and the *IC* of 104.2 $, and both of them are superior to the ACT-RCC terminal [15]. This is because the length of copper pipes of the former is larger and the price of steel panels is less than aluminum-alloy panels. However, the appearance area of the steel-panel RCC terminal is 1300mm (L) × 900 mm (H), which is greater than the ACT-RCC terminal, resulting in more spacious occupation area. Hence, in terms of thermal and economic performances, the steel-panel RCC terminal is suitable to provide enough cooling capacity with low initial cost. In terms of occupation area, the ACT-RCC terminal is a more preferable choice for application in future.

Table 9. The optimization results of the ACT-RCC terminal compared with other structures.

Parameters	Original structure of the ACT-RCC terminal	Optimized structure of the ACT-RCC terminal	Optimized structure of the steel-panel RCC terminal	Unit
copper pipe diameter (D_{co})	6.0	8.7	6.0	mm
copper pipe spacing (Sp_{co})	40.0	25.5	40.0	mm
rib height (H_{rib})	20.0	30.3	40.0	mm
cooling capacity per unit appearance area (Q_{aa})	90.1	104.5	109.8	W
initial cost (*IC*)	147.6	132.9	104.2	$
outline dimension	1600 mm (L) × 650 mm (H)	1200 mm (L) × 650 mm (H)	1300 mm (L) × 900 mm (H)	/

5. Conclusion

A novel heuristic approach is proposed to optimize the thermal and economic performances of the ACT-RCC system, adopting the ANN and MOGA. The numerical and economic models of the ACT-RCC terminal are established and the numerical model is validated by the measured data. Taking the copper pipe diameter, copper pipe spacing and rib height as decision variables, and the cooling capacity and initial cost as objective functions, the optimal solution of this terminal is obtained. The main conclusions are drawn as follows:

(1) The numerical model of the ACT-RCC terminal shows satisfactory agreement with the experimental data. The simulated results of the refrigerant outlet pressure and temperature as well as cooling capacity of this system are within the relative errors of 3.1%, 9.4% and 6.7%, respectively.

(2) The constructed ANN model is able to accurately and quickly predict the thermal and economic performances of the ACT-RCC system. The goodness of fit of the cooling capacity and initial cost are 0.9854 and 0.9631, and the runtimes of them are merely 3.4 s and 1.7 s.

(3) Based on the heuristic optimization approach, the copper pipe diameter with

8.7 mm, copper pipe spacing with 25.5 mm and rib height with 30.3 mm of the ACT-RCC terminal are recommended. The grey relational analysis of the above factors indicates that the rib height has the greatest impact on cooling performance, and the copper pipe diameter as a main contributor for initial cost.

(4) Compared with original structure, the cooling capacity of the improved ACT-RCC system is enhanced by 16.0% and the initial cost is declined by 10%. Moreover, its appearance area is decreased from 1.04 m^2 to 0.78 m^2.

The proposed heuristic optimization approach not only improves cooling performance but also reduces initial cost, which is conductive to solve complex optimization issues of the RCC terminals and further promote its practical application.

Acknowledgements

This work was supported by the National Natural Science Foundation of China (No. 52008290).

References

[1] International Energy Agency, World energy investment, 2021.

[2] Z. Liu, W. Li, Y. Chen, Y. Luo, L. Zhang, Review of energy conservation technologies for fresh air supply in zero energy buildings, Applied Thermal Engineering, 148 (2019) 544-556.

[3] B. Poel, G.V. Cruchten, C.A. Balaras, Energy performance assessment of existing dwellings, Energy and Buildings, 39 (4) (2007) 393-403.

[4] B. Wu, W. Cai, H. Chen, A model-based multi-objective optimization of energy consumption and thermal comfort for active chilled beam systems, Applied Energy, 287 (2021) 116531.

[5] Z. Tian, L. Yang, X. Wu, Z. Guan, A field study of occupant thermal comfort with radiant ceiling cooling and overhead air distribution system, Energy and Buildings, 223 (2020) 109949.

[6] C. Cen, Y. Jia, K. Liu, R. Geng, Experimental comparison of thermal comfort during cooling with a fan coil system and radiant floor system at varying space heights, Building and Environment, 141 (2018) 71-79.

[7] T. Mikeska, S. Svendsen, Study of thermal performance of capillary micro tubes integrated into the building sandwich element made of high performance concrete, Applied Thermal Engineering, 52 (2) (2013) 576-584.

[8] H. Lim, J.-W. Jeong, Energy saving potential of thermoelectric radiant cooling panels with a dedicated outdoor air system, Energy and Buildings, 169 (2018) 353-365.

[9] Q.J. Kwong, S.J. Kho, J. Abdullah, V.R. Raghavan, Evaluation of energy conservation potential and complete cost-benefit analysis of the slab-integrated radiant cooling system: A Malaysian case study, Energy and Buildings, 138 (2017) 165-174.

[10] M.K. Kim, J. Liu, S.-J. Cao, Energy analysis of a hybrid radiant cooling system under hot and humid climates: A case study at Shanghai in China, Building and Environment, 137 (2018) 208-214.

[11] X. Su, L. Zhang, Z. Liu, Y. Luo, J. Lian, Y. Luo, A computational model of an improved cooling radiant ceiling panel system for optimization and design, Building and Environment, 163 (2019) 106312.

[12] J. Joe, P. Karava, A model predictive control strategy to optimize the performance of radiant

floor heating and cooling systems in office buildings, Applied Energy, 245 (2019) 65-77.

[13] M. Ye, A.A. Serageldin, K. Nagano, Numerical optimization of a novel ceiling radiant cooling panel combined with wall attached ventilation system, Case Studies in Thermal Engineering, 26 (2021) 101066.

[14] Y. Xie, P. Hu, N. Zhu, F. Lei, L. Xing, L. Xu, Collaborative optimization of ground source heat pump-radiant ceiling air conditioning system based on response surface method and NSGA-II, Renewable Energy, 147 (2020) 249-264.

[15] T. Jiang, S. You, Z. Wu, H. Zhang, Y. Wang, S. Wei, A novel refrigerant-direct radiant cooling system: Numerical simulation-based evaluation, Applied Thermal Engineering, 198 (2021) 117442.

[16] Z. Li, D. Zhang, X. Chen, C. Li, A comparative study on energy saving and economic efficiency of different cooling terminals based on exergy analysis, Journal of Building Engineering, 30 (2020) 101224.

[17] L.B. Boccardo, O.B. Kazanci, J.Q. Allerhand, B.W. Olesen, Economic comparison of TABS, PCM ceiling panels and all-air systems for cooling offices, Energy and Buildings, 205 (2019) 109527.

[18] K. Zhou, J. Mao, Y. Li, H. Zhang, Performance assessment and techno-economic optimization of ground source heat pump for residential heating and cooling: A case study of Nanjing, China, Sustainable Energy Technologies and Assessments, 40 (2020) 100782.

[19] A. Kusiak, M. Li, Cooling output optimization of an air handling unit, Applied Energy, 87 (3) (2010) 901-909.

[20] P.M. Ferreira, A.E. Ruano, S. Silva, E.Z.E. Conceição, Neural networks based predictive control for thermal comfort and energy savings in public buildings, Energy and Buildings, 55 (2012) 238-251.

[21] M. Imran, N.A. Pambudi, M. Farooq, Thermal and hydraulic optimization of plate heat

exchanger using multi objective genetic algorithm, Case Studies in Thermal Engineering 10 (2017) 570-578.

[22] H. Bagheri-Esfeh, H. Safikhani, S. Motahar, Multi-objective optimization of cooling and heating loads in residential buildings integrated with phase change materials using the artificial neural network and genetic algorithm, Journal of Energy Storage 32 (2020) 101772.

[23] ANSI/ASHRAE. Standard 55: Thermal Environmental Conditions for Human Occupancy, American Society of Heating, Refrigerating, and Air-Conditioning Engineers, Atlanta, GA, 2017.

[24] K.E. Gungor, R. Winterton, A general correlation for flow boiling in tubes and annuli, International Journal of Heat and Mass Transfer, 29 (1986) 351-358.

[25] C. Yao, H. Li, Y. Xue, X. Liu, C. Hao, Investigation on the frictional pressure drop of gas liquid two-phase flows in vertical downward tubes, International Communications in Heat and Mass Transfer, 91 (2018) 138-149.

[26] L. Su, N. Li, X. Zhang, Y. Sun, J. Qian, Heat transfer and cooling characteristics of concrete ceiling radiant cooling panel, Applied Thermal Engineering, 84 (2015) 170-179.

[27] S. Shao, H. Zhang, Z. Liu, S. You, Y. Wang, Thermo-economic optimization of the direct-condensation radiant heating panel: A numerical-based approach, Energy and Buildings, 240 (2021) 110908.

[28] S. Kaviani, I. Sohn, Application of complex systems topologies in artificial neural networks optimization: An overview, Expert Systems with Applications, 180 (2021) 115073.

[29] Nasruddin, Sholahudin, M. I. Alhamid, K. Saito, Hot water temperature prediction using a dynamic neural network for absorption chiller application in Indonesia, Sustainable Energy Technologies and Assessments, 30 (2018) 114-120.

[30] Nasruddin, Sholahudin, P. Satrio, T.M.I. Mahlia, N. Giannetti, K. Saito, Optimization of HVAC system energy consumption in a building using artificial neural network and multi-objective

genetic algorithm, Sustainable Energy Technologies and Assessments, 35 (2019) 48-57.

[31] A.T. Mohammad, S.B. Mat, M.Y. Sulaiman, K. Sopian, A.A. Al-abidi, Artificial neural network analysis of liquid desiccant regenerator performance in a solar hybrid air-conditioning system, Sustainable Energy Technologies and Assessments, 4 (2013) 11-19.

[32] K.M. Reese, Deep learning artificial neural networks for non-destructive archaeological site dating, Journal of Archaeological Science, 132 (2021) 105413.

[33] F. Pourfattah, M. Sabzpooshani, On the thermal management of a power electronics system: Optimization of the cooling system using genetic algorithm and response surface method, Energy, 232 (2021) 120951.

[34] A. Yusuf, N. Bayhan, H. Tiryaki, B. Hamawandi, M.S. Toprak, S. Ballikaya, Multi-objective optimization of concentrated Photovoltaic-Thermoelectric hybrid system via non-dominated sorting genetic algorithm (NSGA II), Energy Conversion and Management, 236 (2021) 114065.

[35] R. Das, D.K. Prasad, Prediction of porosity and thermal diffusivity in a porous fin using differential evolution algorithm, Swarm and Evolutionary Computation, 23 (2015) 27-39.

[36] W. Wang, R. Zmeureanu, H. Rivard, Applying multi-objective genetic algorithms in green building design optimization, Building and Environment, 40 (11) (2005) 1512-1525.

[37] W. Huang, H.N. Lam, Using genetic algorithms to optimize controller parameters for HVAC systems, Energy and Buildings, 26 (3) (1997) 277-282.

[38] M. Aminyavari, B. Najafi, A. Shirazi, F. Rinaldi, Exergetic, economic and environmental (3E) analyses, and multi-objective optimization of a CO2/NH3 cascade refrigeration system, Applied Thermal Engineering, 65 (1) (2014) 42-50.

[39] M.H. Ahmadi, H. Sayyaadi, A.H. Mohammadi, M.A. Barranco-Jimenez, Thermo-economic multi-objective optimization of solar dish-Stirling engine by implementing evolutionary algorithm, Energy Conversion and Management, 73 (2013) 370-380.

Highlights:

1) A novel heuristic approach is proposed to optimize the ACT-RCC terminal.
2) The runtimes of ANN model are 1.21s for cooling capacity and 1.24s for initial cost.
3) The optimal structure is D_{co} with 8.7 mm, Sp_{co} with 25.5 mm and H_{rib} with 30.3 mm.
4) The cooling capacity is enhanced by 16% and initial cost is reduced by 10%.
5) The appearance area of optimum solution is decreased from 1.04 m^2 to 0.78 m^2.